

Facies characterization of organic-rich mudstones from the Chokier Formation (lower Namurian), south Belgium

CHRISTIAN J. NYHUIS¹, DANIEL RIPPEN² & JULIEN DENAYER^{3,4}

¹*Institute of Geology and Mineralogy, University of Cologne, Zùlpicher StraÙe 49a, D-50674 Cologne, Germany. E-mail: chr.nyhuis@googlemail.com*

²*Institute of Geology and Geochemistry of Petroleum and Coal, RWTH Aachen University, LochnerstraÙe 4-20, D-52056 Aachen, Germany*

³*Service de Paléontologie animale et Humaine, Département de Géologie, Université de Liège, Allée du Six Août, Bat. B18, Sart Tilman, B4000 Liège, Belgium*

⁴*School of Earth Sciences, The University of Queensland, Saint Lucia, Queensland 4072, Brisbane, Australia*

ABSTRACT. In a case study of two wells from the Namur Synclinorium, the black shale-dominated Chokier Formation was analyzed for petrography, mineralogy and organic geochemistry. Thin section petrography revealed a different facies assemblage for each well and a total of six microfacies types. Whole rock mineralogical data largely confirms a facies-dependent mineral composition. All different microfacies types of locality 1 (MFT-1, laminated silty mudstone; MFT-2, laminated mud-clast-rich mudstone; MFT-3, calcareous bioclast-rich mudstone) and locality 2 (MFT-4, lenticular mudstone; MFT-5, burrow-mottled mudstone; MFT-6, burrowed silty laminated mudstone) show ample evidence of a distal shelf environment that is sourced by currents, which may be linked to seasonal (monsoonal) transport of sediment from land to sea. Erosive bedload transport is an important mechanism of sedimentation whereas accumulation by settling from the water column can be excluded for the majority of investigated strata. Frequently, endobenthic activity and other processes after deposition, e.g. winnowing and reworking, caused strong fabric modifications. Various, but simple ichnofabrics prove at least temporary dysoxic conditions as confirmed by relatively low TS/TOC ratios. With regard to sedimentary features, organic geochemistry data hints to organic matter preservation due to rapid burial rather than intense anoxia. Silicification is a widespread diagenetic feature independent from facies and locality. It is most likely linked to a high supply rate of terrestrially dissolved silica as indicated by SEM observations, paleogeographic constraints and sedimentary features.

KEYWORDS: Carboniferous, Namur Synclinorium, drill core, black shale, petrography, TOC, XRD

1. Introduction

The sediments of the Belgian Chokier Formation are predominantly marine mudstones and pro-delta shales that originated from the tectonically controlled drowning of an emerged karstified paleotopography (e.g. Dusar, 2006a, 2006b and references therein). The former landscape may be compared to the famous site in Ha Long Bay (Vietnam): paleotopographical highs prevented strong currents or waves to affect the sedimentary basin. Time equivalent organic-rich mudstone dominated successions of the NW European Carboniferous Basin (Kombrik et al., 2008) are the Upper Alum Shale Formation (Eisenberg Formation, Korn, 2006) (Germany), the Epen Formation/Geverik Member (Netherlands), and the Bowland Shale/Edale Shale Formations (United Kingdom). Recently, these deposits are considered as a potential target for unconventional hydrocarbon exploration and thus are experiencing more attention (e.g. Andrews, 2013; Ghanizadeh et al., 2013; Hartwig et al., 2010; Kerschke & Schultz, 2013; Kõnitzer et al., 2014; Littke et al., 2011; Maynard & Dunay, 1999; Uffmann et al., 2012; Van Hulst & Poty, 2008; Van Hulst, 2012). Apart from the study of Uffmann et al. (2012) and Ghanizadeh et al. (2013), scientific interest on the Chokier Formation has been long delayed.

While the sedimentology and mineralogy of paralic, coal-bearing Namurian and Westphalian strata in Belgium are relatively well known (see Paproth et al., 1983; Dusar, 2006a and references therein), available information on the Chokier Formation, i.e. especially petrographic data, restrains on early studies of specific basal layers (Anten & Bellière, 1920; Bellière, 1920). A subsurface facies analysis based upon geophysical wireline logs for the western Campine (northeastern Belgium) (Langenaeker & Dusar 1992) showed that the lower Namurian basin was frequently connected with an open marine environment and later turned into a delta-related system. Interestingly, first geochemical and mineralogical data illustrate similarities in terms of organic carbon content, maturity and silica content, to the Barnett Shale in Texas (Ghanizadeh et al., 2013; Uffmann et al., 2012).

By the example of two wells from the Namur Synclinorium in southern Belgium, this study presents the first stratified

sedimentological data based on thin section petrography. Within the context of organic geochemistry and mineralogical data, we aim to characterize different rock types and to reconsider the depositional environment of this poorly documented mudstone succession.

2. Geological setting

In southern Belgium Namurian rocks crop out in various structural units. Within the Dinant Synclinorium, Namurian strata are known from the deepest synclines, i.e. "basins" in the Belgian literature (Clavier, Anhée, Florennes, and Assesse basin). Moreover, important (temporary) exposures are situated in the Haine-Sambre-Meuse Overturned Thrust Sheets (former southern limb of the Namur Synclinorium), the Brabant Parautochthon (former northern limb of the Namur Synclinorium) (Belanger et al., 2012) and the Vesdre area (Fig. 1). Likewise, Namurian strata are known from sub-surface of the Campine area (northeastern Belgium, summarized by Delmer et al., 2001) as part of the NW European paralic coal basin. The two cores presented within this study were drilled in the former 'Namur Synclinorium'. Locality 1 (Fig. 1) is situated in the Brabant Parautochthon, within the Andenne area. Locality 2 belongs to the Haine-Sambre-Meuse Overturned Thrust Sheets (HSM OTS in Fig. 1) west of Liège.

Within the 'Namur Synclinorium', the 20 to 40 m-thick Chokier Formation is devoid of coal-seams (Delmer et al., 2001). Associated rocks are described as fissile and fossiliferous organic-rich shales, commonly referred as «ampélites» within classic Belgian literature (for summary see Dusar, 2006a, 2006b; Delmer et al., 2001). These shales are occasionally calcareous, aluminiferous, and individual beds may be silicified («phtanites»). Thickness increases towards the South (Dinant Synclinorium) where first coal-seams are developed much earlier in the sequence (Bois-et-Borsu Member). Westward the Chokier Formation reaches up to 200 m in the Saint-Ghislain borehole (Mons area, westernmost part of the Namur Synclinorium) (Fig. 1) where it finally is laterally replaced by siliceous shales of the Gottignies Formation (Delmer et al., 2001). In the vicinity of Visé (Fig. 1), the Chokier Formation overlies the uppermost Viséan to lowermost Namurian Souvré Formation that is dominated

microfacies types, representative samples were analyzed for vitrinite reflectance, SEM, XRD, TOC and TS. Each analysis has been carried out on identical samples, respectively to ensure its affiliation to the particular microfacies type.

3.1 Petrography

Altogether 33 large (75 mm x 100 mm) thin sections from 17 samples of locality 1 and 32 thin sections from 20 samples of locality 2 were examined by binocular and petrographic microscope. Stabilizing of fissile mudstones was achieved using epoxy resin (RECKLI-Injektionsharz EP) prior to slabbing and thin section preparation. Thin section samples were cut with a water-cooled diamond-saw. After drying (48 hours, 60°C) samples were polished with a mixture of grinding powder (silicon-carbide of 600 µm grain-size) and water. After drying again (48 hours, 60°C), samples were mounted (Araldite 2020) on glass plates. 72 hours later samples were ground down again to their final thickness. Neither ethanol nor oil was used.

SEM-samples were broken perpendicular to bedding and grinded prior to edge-milling (GATAN Iliion ion mill) in order to achieve a smooth sample surface. Uncoated samples were viewed on surfaces perpendicular to bedding by an electron microscope (FEI Quanta FEG 400) with EDS for mineral identification.

Vitrinite reflectance measurements were performed on polished sections. General information on vitrinite reflectance analysis and organic petrography are described by Taylor et al. (1998). Within our work we follow the protocol and the specifications for the laboratory conditions at RWTH Aachen University described by Sachse et al. (2011) and Littke et al. (2012). The microscope setup was calibrated with standards of known reflectances: yttrium–gallium–garnet (0.889%) and gadolinium–gallium–garnet (1.721%). A minimum of 50 measurements per sample were performed to achieve statistically valid values. To reach this amount of data points for samples with insufficient amounts of vitrinites, reflectance values were calculated from measured bitumen reflectance data following the equation

$$VR_r = (BR_r + 0.2443) / 1.0495 \text{ from Schoenherr et al. (2007).}$$

3.2 X-Ray Diffraction

One part of each sample was gently crushed and mixed with 30% acetic acid for three days. After calcitic cement dissolution, residual material was washed by centrifuging. To achieve a suspension of the clay fraction, distilled water and ammonia was added to the sample material and subsequently placed in an ultrasonic bath for 30 minutes. The clay suspension was centrifuged to deposit the entire < 2 µm fraction, which was filtered onto unglazed ceramic tiles. Another part of the sample was powdered by a McCrone Micronising Mill. Industrial methylated spirits were used to minimize structural grinding damage. A few drops of the resulting slurry were dried on a silicon wafer.

The instrumental setup was a Siemens PSD X-ray diffractometer using Ni-filtered CuK α radiation. Clay tiles were scanned using a 0.02° step width, with 0.2 mm slits from 2 to 40° 2 θ . The tiles were scanned again after treating with glycol, after heating at 400°C for 4 hours, and after heating at 550°C, also for 4 hours. The whole rock powder samples were scanned with a 0.02° step width, and 0.2 mm slits, from 5 to 70° 2 θ .

The software Macdiff was used to deconvolute the peak areas. Relative mineral amounts were then calculated from the areas of their according peak areas in relation to measured standards of known compositions.

3.3 Total organic carbon (TOC) and total sulfur (TS)

Determination of the total organic carbon (TOC) was conducted with two different setups. The majority of samples were analyzed with a Leco SC-632 combustion oven after removal of carbonate using diluted HCl. The CO₂ released by combustion of organic compounds was measured using an infrared detector. Based upon these measurements, the organic carbon content of samples was calculated.

Some additional samples were measured using an Elementar LiquiTOC II with a solid phase module. Untreated, crushed

rock samples were used with this setup. CO₂ concentrations from combustion of rock sample were measured by an infrared detector. Cross-checking TOC values of 3 samples measured on both setups showed very good accordance, i.e. a deviation of less than 5% for the results from the Leco SC-632 and the Elementar LiquiTOC II. Due to the preparatory procedures used in the different setups, total inorganic carbon from, e.g. calcite, could only be measured for the untreated samples.

Total sulfur (TS) analysis was performed on all samples with a Leco S200 combustion oven at a temperature of 1800°C under oxygen atmosphere. The released SO₂ concentrations were recorded by an infrared detector.

4. Results and Discussion

4.1 Lithostratigraphy and Mudstone microfacies types of locality 1

The Chokier Formation exposed within the core of locality 1 disconformably overlies mid-Viséan carbonates (oolithic grainstone and bioclastic packstone/floatstone) of the Seilles Member (Fig. 3A). The 2.8 m thick basal deposits of the Chokier Formation are composed of matrix supported breccia (argillaceous siltstone and limestone fragments), argillaceous siltstone and sandstone. With regard to their thickness and rubble appearance within the core a certain anthropogenic influence, possibly due to abandoned mining in this area, is assumed. On top of this accumulation the Chokier Formation is composed of a 26.7 m thick heterogeneous mudstone dominated succession. The strata can be subdivided in two units. The lower unit (35.50 m – 25.16 m) is dominated by silty mudstone followed by an upper unit (25.16 m – 8.80 m) dominated by dark mudstone and carbonate-rich dark mudstone. Macrofossils are restricted to the upper unit and include common plant remains, e.g. *Calamites*, bivalves and goniatites.

Based on mineralogy, fabric and texture we have defined three mudstone facies types: i.e. laminated silty mudstone (MFT-1); laminated mud-clast-rich mudstone (MFT-2); and calcareous bioclast-rich mudstone (MFT-3).

4.1.1 Laminated silty mudstone, MFT-1 (Fig. 4A; Fig. 4B; Fig. 8A)

This facies is characterized by a millimeter-scale alternation of graded clay/silt couplets. Boundary diffusion and sharp erosional contacts between individual laminae can be observed. Rare *Planolites* and vertical biodeformational structures up to 5mm in diameter (Fig. 4A) are the most conspicuous signs of infaunal activity. The latter, in some cases, cause a mottled fabric within some horizons. Common vertical biodeformational structures are differentiated from dewatering structures, which are another typical feature for the laminated silty mudstones facies by upward branching, vertical channels with a variable diameter (0.2 – 0.7 mm) and a three-dimensional expansion seen in hand specimens. Fine dispersed authigenic pyrite crystals are common. In some cases, they are enriched in small lenses ranging from 0.3 mm to 0.6 mm (Fig. 4B). The detrital silt grains, i.e. quartz and a few feldspars of MFT-1 are angular and poorly sorted (Fig. 4B). MFT-1 is frequently silicified. Silicification is expressed by fine silt-sized opaline silica crystals and silt to sand-sized detrital grains with authigenic silica overgrowth. Distribution within the matrix is homogeneous.

Interpretation. – A distal pro-delta setting that favors high input of fine siliclastic material is regarded as the depositional environment for MFT-1. High sedimentation rates are witnessed by dewatering structures. They frequently disrupt alternating silt/clay laminae. Omnipresent boundary diffusion reflects cryptic bioturbation (Pemberton et al., 2008) and thus indicates meiofaunal activity under at least temporary dysoxic conditions immediately after deposition. Due to high sedimentation rates, time available for infaunal activity to destroy the primary fabric was insufficient. Moreover, rapid infaunal colonization is reflected by the presence of vertical biodeformational structures. They are generated within water-saturated, soupy sediments and show a characteristic indistinct outline (Wetzel, 1983; Wetzel & Uchmann, 1998). These conditions prevailed within a short time range shortly after deposition prior to subsequent expulsion by

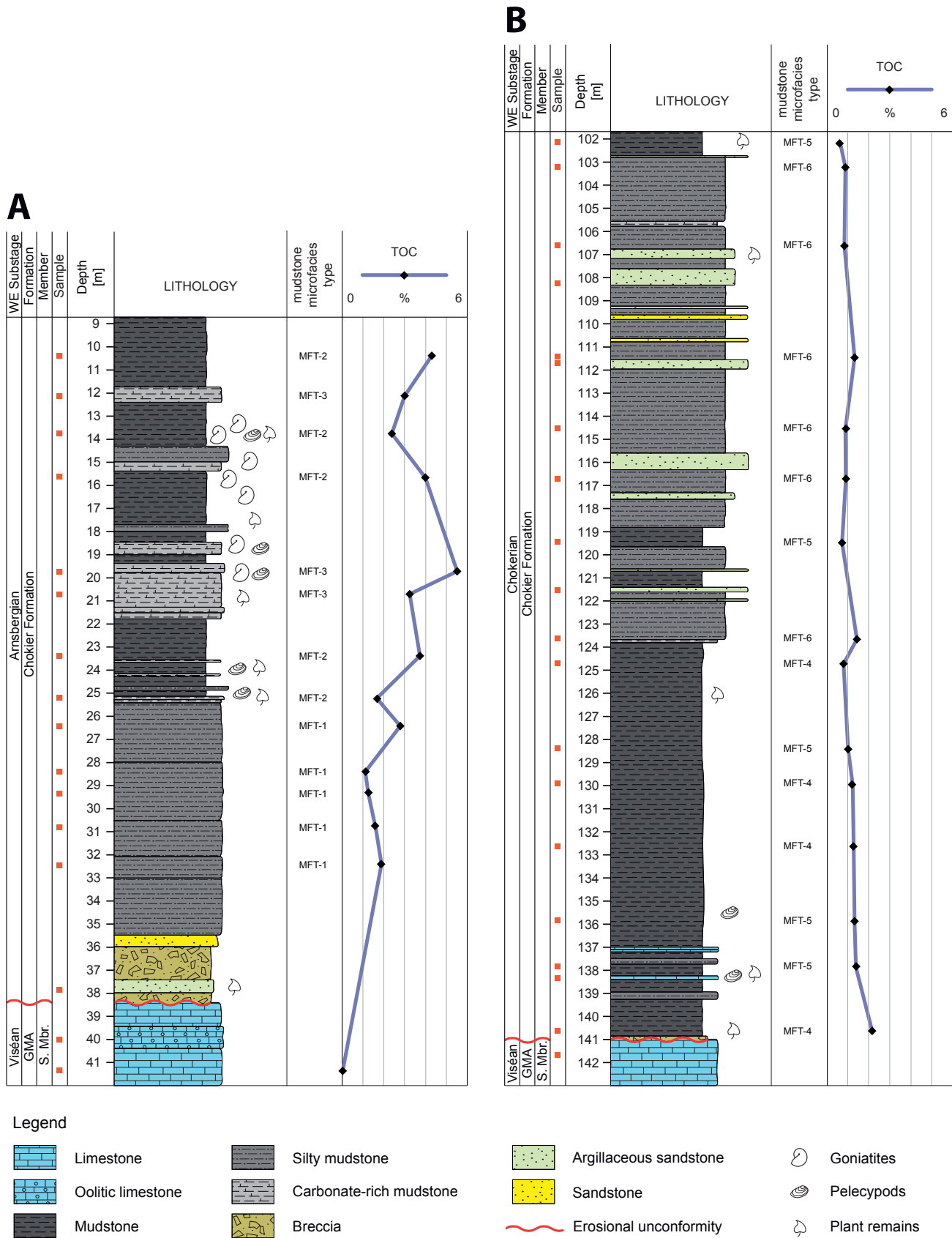


Figure 3. Lithological pattern with corresponding mudstone facies types (see 4.1; 4.2) and TOC data of locality 1 (A) and locality 2 (B) (see 4.3). Abbreviations: GMA: Grands-Malades Formation; S. Mbr.: Seilles Member.

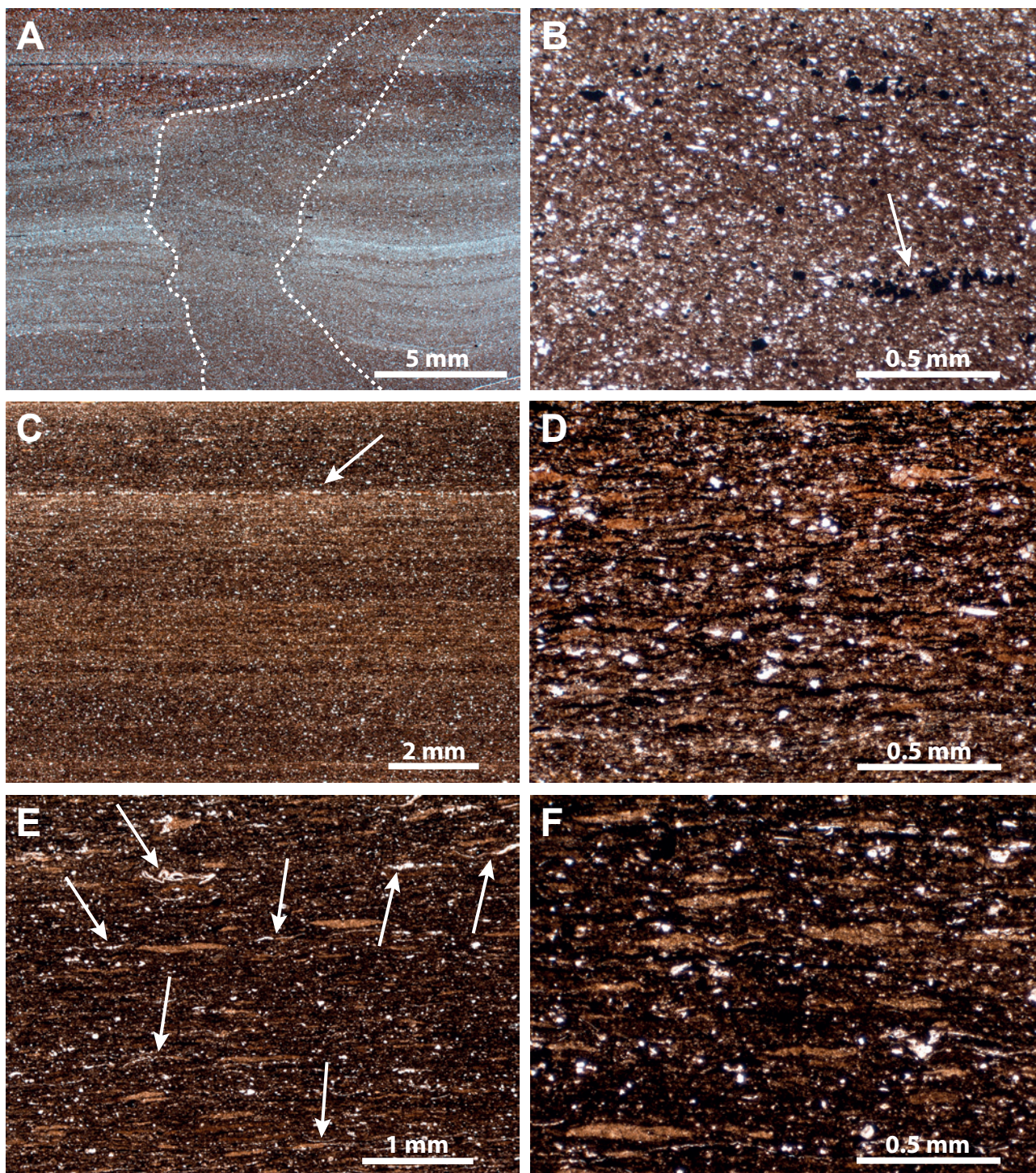


Figure 4. Photomicrographs of mudstone microfacies types of locality 1. All views are perpendicular to bedding. A: Example of a laminated silty mudstone (MFT-1). Biodeformational structure indicated by dashed line indicates “soupy” conditions when the structure was generated (depth: 32.33 m). B: Detail of A, showing high amount of fine detrital grains embedded in a clay-rich matrix. Note small dark lense (arrow) that is mainly composed of pyrite grains. C: Example of a laminated mud-clast-rich mudstone (MFT-2). Uppermost lamina showing basal lag (arrow), composed of fine detrital grains. Diffuse boundaries most likely are the result of infaunal activity (depth: 15.6 m). D: Detail of C. The detail shows numerous flattened and partially amalgamated silt/clay clasts (brownish) and a moderate amount of detrital grains. E: Example of a calcareous bioclast-rich mudstone (MFT-3). The faintly laminated fabric of this mudstone facies shows numerous flattened silt/clay-clasts (bright brown). Some fine calcareous bioclasts highlighted (arrows) (depth: 20.69 m) F: Detail of E highlights the poorly sorted brownish silt/clay-clasts within a clay rich matrix.

surcharge. In contrast, times of reduced sediment supply under low energy conditions are reflected by minor occurrences of *Planolites* burrows that require relatively firm substrates.

4.1.2 Laminated mud-clast-rich mudstone, MFT-2 (Fig. 4C; Fig. 4D; Fig. 8B)

This facies is characterized by a nearly lenticular fabric, caused by dense packing of poorly sorted silt/clay lenses. They are embedded within a clay-rich matrix (Fig. 4C). Well-developed fine lamination is the result of bedding parallel submillimeter-scale variations in the lense/matrix ratio. Rarely, very fine calcareous

bioclasts, i.e. filamentous bivalve shells and bioclasts of uncertain origin can be observed. Thin silt laminae may separate layer contacts (Fig. 4C) and commonly show prominent boundary diffusion. Evidence of large burrowing organisms is lacking. In many cases, a minor to moderate silicification or dolomitization is developed. The latter is represented by one sample that shows well-developed fine silt-sized rhombohedral dolomite crystals embedded within a dark clay-rich matrix. Dolomite is dominated by Fe-dolomite (see 4.4). Silicification in thin section is expressed by homogeneous distributed fine-silt-sized opaline silica crystals and detrital grains that show silica overgrowth.

Interpretation. – An accumulation due to erosive bedload transport is most likely for this facies rather than being largely settled from slow-moving currents or suspension. Erosive conditions are indicated by thin silt laminae that separate different layers. These laminae are the result from winnowing of the relatively silt-rich muddy sediment. The poorly sorted silt/clay lenses in fact are highly flattened, mud-clasts. Flume studies show that these clasts are the result of intermittent erosion and bedload transport of water-saturated mud (Schieber et al., 2010). They can be found within other mudstone facies types of the Chokier Formation as well (see 4.1.3; 4.2.1). Regarding the very fine lamination, which is a result of erosive bottom currents, variations in the clast/matrix ratio reflect fine-scaled reworking or winnowing of material. However, changing flow velocities and corresponding changes in sediment load may also have influenced the fabric. Minimum oxygen content is supported by diffuse lamination, caused by meiofaunal activity, e.g. nematodes.

4.1.3 Calcareous bioclast-rich mudstone, MFT-3 (Fig. 4E; Fig. 4F)

A moderate amount of flattened, light colored, silt/clay lenses and a minor to moderate content of fine calcareous bioclasts within a clay-rich matrix (Fig. 4E) characterizes MFT-3. Fossil components include disarticulated, thin-shelled ostracodes and bivalves. Minor amounts of dispersed fine silt-sized angular quartz grains can be observed within this facies. In some cases, bioclasts are arranged in thin layers, which commonly show lamina disruption. Parallel arrangement of poorly sorted lenses that are composed of a mixture of silt and clay results in a faintly to indistinct laminated fabric (Fig. 4F). MFT-3 may be similar to the likewise lense-bearing MFT-2. However, MFT-3 shows a significantly lower amount of lenses. Despite the well-developed lamination, main features that separate MFT-2 from MFT-3 are (1) the denser packed lenses, (2) a slightly elevated silt-sized quartz content (Fig. 4D), and (3) a significantly lower amount of fine bioclasts that are never arranged in laminae.

Interpretation. – Observed sedimentary features are consistent with deposition by turbidity currents occurring at great distances from the sediment source (Piper & Stow 1991). In these deeper and more distal areas, most of the coarser grained material had dropped out of the flow, leaving only very fine-grained sediment and components of low volumic mass, e.g. water-saturated mud-clasts and thin-shelled fossils. The relatively high amount of fine-grained bioclasts within MFT-3 has been derived from adjacent shallow marine settings and upper-slope settings. Disarticulation and fragmentation of fossil components underlines exclusion of deposition by pelagic rain. The poorly sorted silt/clay lenses are transported mud-clasts (see 4.1.2) and indicate a certain flow regime as well. Lamina disruption of intercalated bioclastic laminae and the faintly laminated fabric is the result of bioturbation. Concluding that this indicates infaunal activity under a dysoxic regime, MFT-3 witnesses a distal, current-driven deposition. It may be linked to seasonal transport of sediment washed away from the land surface to sea, and subsequent fabric modifications by infaunal activity.

4.2 Lithostratigraphy and Mudstone microfacies types of locality 2

The Chokier Formation exposed within the core of locality 2 disconformably overlies mid-Viséan carbonates (brachiopod-rich floatstone) of the Seilles Member (Fig. 3B). On top of a 5 cm thick bed of matrix supported basal breccia (limestone and partly reddened sandstone fragments), the Chokier Formation is composed of a 39 m thick heterogeneous mudstone succession. It can be separated in two units. The lower unit is dominated by dark mudstone (141.00 m – 124.18 m), the upper unit (124.18 m – 102.0 m) by gray silty mudstone and argillaceous sandstone. Macrofossils are rare and restricted to small plant fragments and bivalves.

Based on mineralogy, fabric and texture we have defined three mudstone facies types: i.e. lenticular mudstone (MFT-4); burrow-mottled mudstone (MFT-5); and burrowed silty laminated mudstone (MFT-6).

4.2.1 Lenticular mudstone, MFT-4 (Fig. 5A; Fig. 5B; Fig. 8C)

A moderate to high amount of light colored and poorly sorted silt/clay lenses within a clay-rich matrix characterizes this

facies (Fig. 5A). The lense/matrix ratio is alternating within a bedding parallel millimeter to centimeter-scale and results in a well-developed lamination (Fig. 5B). Lower and upper boundaries are either diffuse or sharp. A minor amount of fine detrital quartz silt is evenly dispersed throughout every layer and never shows enrichments within lamina. Fossil content is represented by moderate amounts of agglutinated foraminifera. They are restricted to clay-rich laminae that commonly show a homogenized fabric. The majority of shells are unbroken, diagenetically compressed and pyrite-filled. In some cases, horizons are enriched with pyrite aggregates (0.2 – 2.0 cm) that always show differential compaction.

Interpretation. – Comparable to MFT-2, MFT-4 is highly influenced by erosion and bedload transport of mud. Erosion is reflected, among others, by sharp surfaces that scour into the underlying lithology (see Fig. 5A). Moreover, erosion of soft mud and subsequent bedload transport is reflected by numerous silt/clay clasts (see Schieber et al., 2010). Their deposition, diagenetic compaction and dense packing cause the lenticular fabric (Schieber et al., 2010), which characterizes MFT-4. In contrast to MFT-2, it shows significantly more clasts. Examples of lenticular mudstone fabric are known from Proterozoic (Banerjee et al., 2006; Schieber et al., 2007), Paleozoic (Davies et al., 2012; Gabbott et al., 2010; Könitzer et al., 2014), Mesozoic (Macquaker et al., 2010; Trabucho-Alexandre et al., 2012) and Cenozoic (Schieber et al., 2007) successions. Thus, it is a common feature within fine-grained systems. Reproduction of lenticular mudstone fabric under laboratory conditions was achieved by flume studies (Schieber et al., 2010) and proves the existence of a flow influenced regime. Bedding parallel variations in the clast/matrix ratio are caused by changing flow velocities and sediment load. Extensive transport is excluded for the clay-rich laminae. They are regarded as deposits that settled from slow-moving currents that are too slow to transport silt/clay clasts, or from suspension. These times of reduced sediment supply provided enough time for infaunal colonization (compare 4.1.1). The common occurrence of unbroken benthic agglutinated foraminifera within those homogenized clay-rich laminae indicates an in-situ embedding under minimum oxygen conditions. This is supported by the fact that agglutinated foraminifera have been reported from several dysoxic black shale accumulations (e.g. Macquaker et al., 2010; Milliken et al., 2007; Nyhuis et al., submitted; Schieber, 2009). However, the majority of MFT-4 lacks homogenized clay-rich laminae, and is influenced by mud-clast loaded currents. They winnowed and eroded the underlying sediment, leaving sharp, scouring boundaries and an overall lenticular fabric (see Fig. 5A, Fig. 5B). Short periods of infaunal activity by soft bodied organisms adapted to quasi-anoxic conditions, caused the observed boundary diffusion.

4.2.2 Burrow-mottled mudstone, MFT-5 (Fig. 5C; Fig. 5D)

This facies is characterized by a clay-rich mottled fabric. *Planolites* and vertical burrows are common features of infaunal activity. Burrow fills show a different contrast and are commonly finer than the surrounding sediment (Fig. 5C). Internal fabric is homogeneous and *Planolites* in particular may be enhanced by a contrast-rich pyritization of its sediment fill. In some cases, indistinct lamination is indicated by slightly coarser and brighter layers (Fig. 5C). These layers essentially show disruption of laminae, erosive boundaries and a homogeneous internal fabric. Mineral composition and faunal content of MFT-5 is comparable to MFT-4 (see 4.2.1). Likewise, it shows minor amounts of fine detrital quartz silt, pyrite aggregates and pyrite-filled shells of complete agglutinated foraminifera (Fig. 5D) that occur more abundantly than in MFT-4.

Interpretation. – The characteristic mottled fabric of MFT-5 is the result of intense bioturbation of MFT-4 in times of reduced sediment supply and increased oxygen conditions. As already illustrated for MFT-4 and MFT-1, time is a limiting factor for infaunal activity within current-influenced environments because the extent sedimentary structure is altered depends on the ratio of biological mixing rate to sediment accumulation rate (Blatt, 1992). Thus, a lowered sediment supply provides sufficient time for burrowing organisms to colonize the seafloor and modify the fabric. Moreover, the abundant occurrence of agglutinated

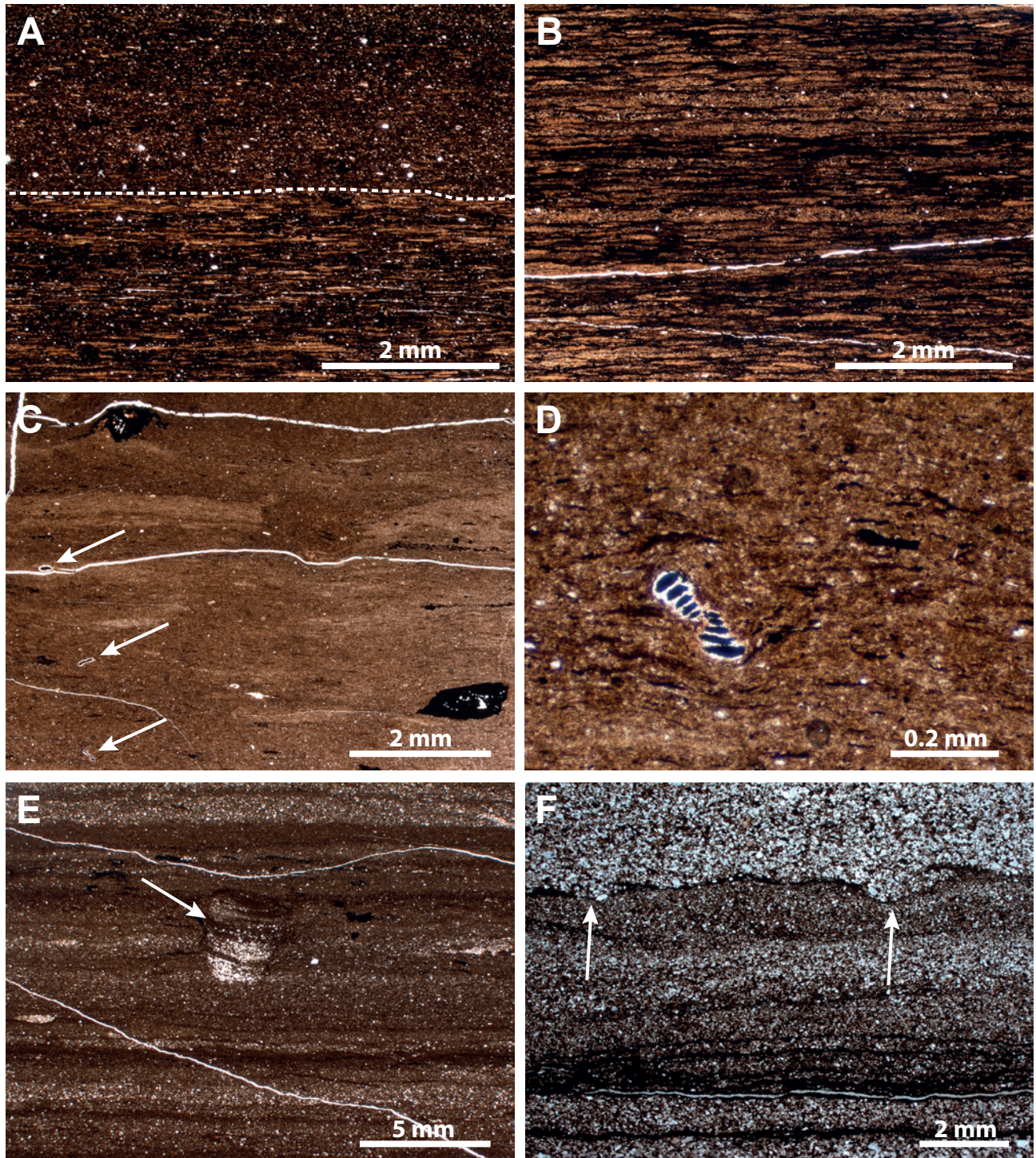


Figure 5. Photomicrographs of mudstone microfacies types of locality 2. All views are perpendicular to bedding. Bright linear voids are preparation artefacts. A: Example of a lenticular mudstone (MFT-4), showing a faintly laminated fabric. Dashed line indicates position of a slightly undulating erosional surface that scours into the underlying lithology (depth: 140.6 m). B: Another example of MFT-4. Note the dense packing of lenses that are conspicuously larger than in A (depth: 132.66 m). C: Example of a burrow-mottled mudstone (MFT-5) with agglutinated foraminifera, some highlighted by arrows. The black spots in the upper left and lower right are pyritized burrows. Note layered sedimentary fabric prior to complete destruction by burrowing and disruption of laminae throughout (depth: 128.4 m). D: Detail of C, showing a pyrite-filled, diagenetically broken benthic agglutinated foraminifer that are abundant within this sample. E: Example of a burrowed silty mudstone (MFT-6). The laminated fabric is cut by a *Teichichnus* trace (arrow) (depth: 114.54 m). F: Fine-grained sandstone layer on top of a mudstone of MFT-6. Note ball & pillow structures and loading at the base of the sandstone layer (arrows) (depth: 111.74 m).

foraminifera within MFT-5 and the trace fossil assemblage, i.e. *Planolites* and vertical burrows, reflect a setting under at least dysoxic conditions. Horizons that show a fabric prior to complete bioturbation, i.e. indistinct lamination, require some consideration. These indistinct laminae lack any flattened silt/clay clasts, a characteristic feature of MFT-4. Consequently, the indistinct and homogenized laminae do not reflect any primary fabric of MFT-4. Regarding the homogenized fabric and the intense bioturbation within MFT-5 they apparently resemble completely bioturbated and redeposited sediment. The apparent similarities of MFT-5

to MFT-4 in biogenic and non-biogenic components show that both facies types partly comprise a common genetic history. With regard to their small-scale alternation within the observed core (see Fig. 3B), MFT-5 represents conditions after invasion of MFT-4 by burrowing organisms in times of increased oxygen concentrations and reduced sediment accumulation rates. Apart from data obtained by thin section petrography, this is supported by different TS/TOC ratios and similar whole rock mineral composition (see 4.3.2; 4.4.2).

4.2.3 Burrowed silty laminated mudstone, MFT-6 (Fig. 5E; Fig. 5F; Fig. 8D)

This facies is characterized by alternating silt- and clay-rich laminae that are cut by infaunal deposit feeding structures (Fig. 5E). It usually is interbedded with thin cross-laminated silt laminae that may show slump-like, soft-sediment deformational structures. The fabric is diverse and ranges from well-laminated to burrow-mottled. Burrow-mottled fabric of silt-rich horizons shows clay-filled *Planolites* burrows. Burrows within well-laminated clay-rich horizons are represented by *Planolites* and *Teichichnus*. The latter shows characteristic curved spreiten arrangement that are pronounced by spreiten-parallel silt-enrichment (Fig. 5E). Apart from these well-visible traces, the simple, low diverse trace-fossil suite commonly consists of diffuse lamination and disruption of laminae. Fossils are restricted to a single finding of a broken and clay-filled agglutinated foraminifer. The burrowed silty mudstone facies is frequently intercalated with fine grained argillaceous sandstones layers. Their thickness is highly variable and ranges from centimeter to decimeter scale. Characteristically, they contain a minor content of very fine calcareous debris. Basal scouring and ball-and-pillow structures are observed at contacts to underlying clay-rich horizons (Fig. 5F). Internally, the sandstone layers may show slump-like, soft-sediment deformational structures that cause a flaserly appearance.

Interpretation. – This facies is the result of event deposition under relatively oxic conditions. Cross-laminated silt layers within clay-rich sections indicate bedload transport by migrating silt ripples. In contrast, dominance of ripple-free, thick argillaceous sandstone layers reflects a different depositional mechanism. Ball-and-pillow structures rather indicate rapid deposition by single sheds than bedload transport. According to Knaust (2002) rapid loading and subsequent dewatering due to deposition of turbidites is a common process. Considering the predominance of highly water saturated soft substrate they provoke formation of ball-and-pillow structures. Lamina diffusion and disruption of laminae are caused by infaunal activity. Moreover, benthic colonization by larger organisms is reflected by simple sediment feeding structures such as *Planolites* and *Teichichnus*. Both are common trace fossils of mudstones (Wetzel & Uchmann, 1998). *Planolites*, whose tracemaker uses oxygen from pore water, indicates oxygenated sediments in shallower tiers (Rodríguez-Tovar & Uchman, 2010). In addition, *Teichichnus*, a rapidly adjusted structure (MacEachern et al., 2009) indicates events of high-energy sediment accumulation (Hovikoski et al., 2008; MacEachern et al., 2009) and is in need of minimum oxygen content as well. As a representative of the *Cruziana* ichnofacies (Seilacher, 1967) it commonly occurs in mid and distal environments below normal wave base. Comparable to MFT-5 (see 4.2.2) sediment accumulation rates were highly variable.

This is expressed in a variable biogenic fabric modification and underlines the episodic sedimentary input: due to reduced sediment accumulation rate (Blatt, 1992) time was sufficient to destroy the primary fabric, which ends up in a mottled fabric within clay-dominated horizons. Deposits that reflect increased sedimentation rates lack those modifications due to rapid burial of endobenthic fauna.

Considering the sedimentary features and the high amount of coarse grained intercalations, i.e. argillaceous sandstones (see Fig. 3B), a delta related system though still distal, is assumed for MFT-6. With regard to the episodic nature of the sediment input a seasonal (monsoonal) influence is most likely. The dominance of MFT-6 in the upper part of locality 2, which has a Chokierian age, might reflect the gradual transition to the paralic and coal-bearing Andenne Formation.

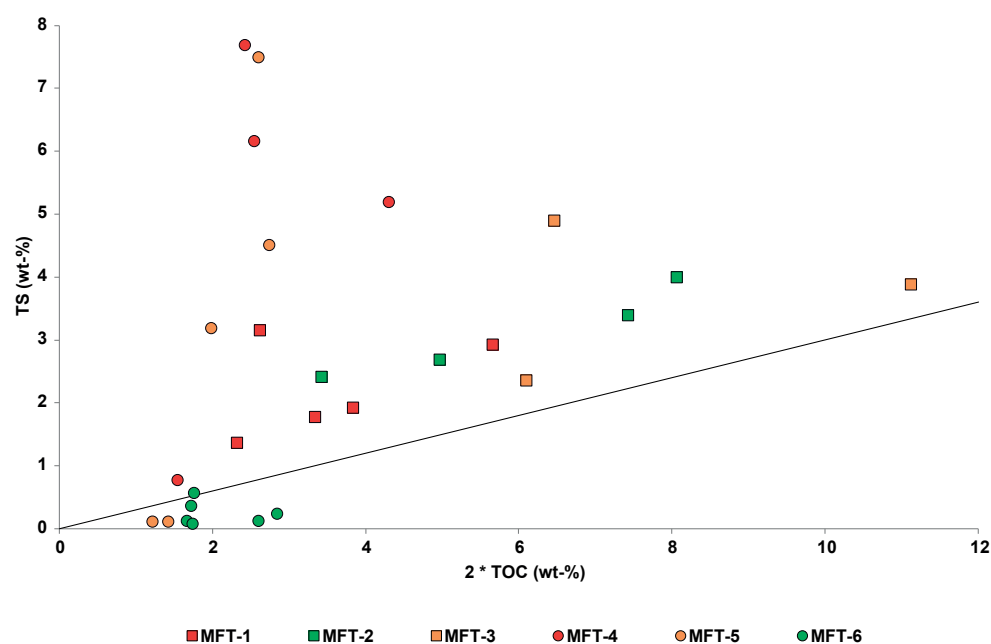
4.3 Organic Geochemistry

The elemental organic geochemical analyses of the two cores reveal significantly different characteristics for each locality in terms of organic carbon content (TOC). Overall, the samples from locality 1 show a wide distribution of TOC values ranging from 1.2% to over 5.6%. Highest TOC values correlate with occurrence of goniatites that in turn correlate with occurrence of MFT-2 and MFT-3 (Fig. 3A). Goniatites indicate fully marine conditions that are the result of high sea level, which favors enhanced organic matter productivity and lowered sedimentation rates. This leads to TOC accumulation by reduced dilution of siliciclastic material. The samples from locality 2 show a more uniform pattern across the sampled interval with values from 0.6% to 2.2% with an average of 1.1% TOC (Fig. 3B).

Large excursions of vitrinite reflectance values (see Muchez et al., 1987) have not been observed and both sample suites show high values of 2.2% on average for the samples of locality 1 and 2.0% for locality 2. Considering these values and by assuming that the Chokier Formation is a marine, type II source rock (due to organic petrographical and elemental geochemical features, see Uffmann et al., 2012), it can be suggested that half of the organic carbon was lost due to maturation, hydrocarbon generation and expulsion (Uffmann et al., 2012). Such a loss in TOC due to maturation is well known from the *Posidonia* shale, which is a Toarcian marine source rock comprising type II kerogen (Rullkötter et al., 1988). The assumed type II source rock characteristics for the Chokier Formation include that marine planktonic and bacterial remains are the source of organic matter. However, terrestrial input (plant remains) have contributed certain proportions of organic matter as well.

To assess TOC contents during deposition in relation to normal marine conditions (Berner, 1984), the measured TOC contents have been multiplied by a factor of 2 (Fig. 6).

Figure 6. Total sulfur (TS) versus total organic carbon (TOC) (multiplied by 2) contents for the different mudstone facies types (“normal marine” line after Berner, 1984). See 4.3 for details.



The total sulfur (TS) values vary in accordance to the TOC contents with the same trends within the succession of locality 1. These values range between 1.4% and 4.9% TS. For locality 2, the results from total sulfur analyses show distinct suites with generally low values of around 0.5% in the upper half of the succession and very high values of up to 7.7% in the lowermost intervals.

The total organic carbon and total sulfur contents strongly depend on the lithological framework and oxygenation state during deposition (Tourtelot, 1979; Berner, 1984). Under normal conditions, TS contents of sediments are buffered by the amount of lead TOC, resulting in a strong correlation between TS and TOC. TS values varying from this correlation line are either enriched or depleted in sulfur. High amounts of sulfur are linked to bacterial sulfate reduction due to dysoxic to anoxic conditions, while sulfur depletion hints to high oxygenation stages. This causes the biodegradation of organic matter. Therefore, each microfacies type described above show characteristic TS/TOC ratios (Fig. 6). For locality 2, the geochemical fingerprints are more diverse in relation to those from the material of locality 1.

4.3.1 Organic geochemical facies characteristics of locality 1

MFT-1 is geochemically characterized by mediocre TOC and TS values, showing TS/TOC ratios of around 1.0 and generally low TOC values. Although anoxicity is inferred from Fig. 6, findings of cryptic bioturbation partly object this assumption (see 4.1.1). Nevertheless, it is assumed that dysoxic conditions have established shortly after deposition due to high sedimentation rates and rapid burial, leading to increased TS resulting from bacterial sulfate reduction. These high sulfur contents are underlined by findings of up to 5% pyrite in the XRD measurements.

Generally dysoxic conditions are assumed for MFT-2 due to varying TOC contents but generally high TS content. The TS/TOC ratios scatter around 1.0 leading to the interpretation of bacterial sulfate reduction buffered by the amount of organic matter input. The scarcity of burrowing benthic organisms supports this observation (compare 4.1.2). Higher pyrite contents (up to 11%) than those of MFT-1 also hint to a high activity of sulfate reducing bacteria.

MFT-3 shows distinct features of bioturbation, leading to the interpretation of dysoxic or higher oxygenated stages for the uppermost sedimentary column (see 4.1.3). The geochemical data reveal oxygen depleted states prevailing after the deposition due to the highest TOC and TS values in the succession, although TS/TOC ratios are partly as low as 0.7. With regard to sedimentary features, TS/TOC ratios hint to organic matter preservation due to rapid burial. Thus, organic matter preservation is assumed to be linked with sedimentation rate, rather than extensive anoxicity.

4.3.2 Organic geochemical facies characteristics of locality 2

MFT-4 shows very high TS/TOC ratios, indicative for extensive dysoxic to anoxic conditions, although TOC contents are only moderate. Such high TS contents hint to oxygen depletion in the lowermost water column above the sediment surface. A quite large scatter in TS/TOC ratios is underlined by varying findings of 2 up to 11% pyrite in the XRD measurement, leading to the suggestion of alternating oxygenation stages, supported by thin section petrography (see 4.2.1).

MFT-5 nearly resembles the geochemical signal from MFT-4. Occasionally the system turned completely oxic, as inferred by few very low TS/TOC ratios and a large scatter of pyrite from 0 up to 9%. Considering the small scaled alternation of MFT-4 and MFT-5 (Fig. 3B) these changes in oxicity gain significant importance in terms of biota and fabric (see 4.2.1; 4.2.2).

MFT-6 represents the most oxygenated geochemical microfacies type of the investigated Chokier Formation. As inferred from thin section petrography (see 4.2.3), these sediments were deposited during events with high sedimentation rates. As Berner (1984) states, such events are one of the processes to introduce oxygen into the sedimentary column, reflected by the low TS/TOC ratios for this microfacies type in Fig. 6. Nevertheless, initial TOC contents for this microfacies type are moderate (ca. 2%), hinting to organic matter preservation due to high sedimentation rates.

4.4 Mineralogy

The mineralogical data obtained in this work are depicted in a ternary diagram, which effectively shows a clustering of data points (Fig. 7). Like organic geochemical composition (see 4.3),

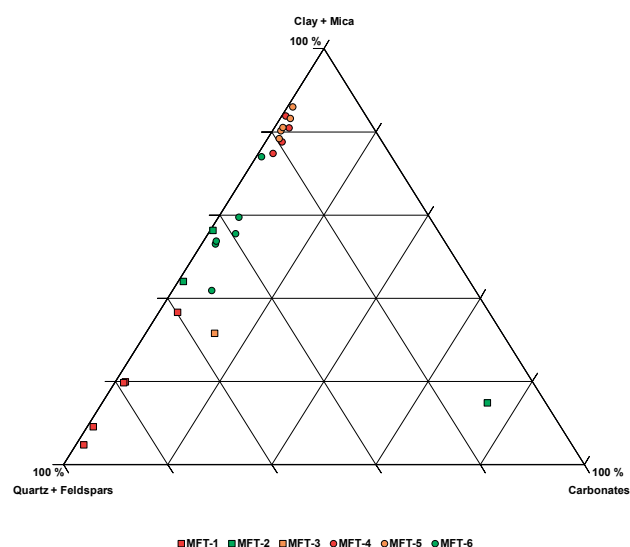


Figure 7. Bulk mineralogy of the different mudstone facies types according to XRD data. See 4.4 for explanations.

samples from locality 1 show characteristic mineralogical features that are significantly different from the samples of locality 2.

4.4.1 Mineralogical facies characteristics of locality 1

MFT-1 is dominated by an unusually high quartz content of up to 90% and an average value of 76%. Furthermore, this facies type is characterized by generally low carbonate contents (< 3%) and varying clay contents (Fig. 7). The clay composition consists mainly of illite/mica and chlorite values are low (< 3%). Smectites were not identified, suggesting the high maturity of the samples. The minor amount of carbonates found in the sample is mainly siderite (c. 1%) with traces of calcite. The high quartz contents of this microfacies type cannot be solely explained by high input of detrital material. Secondary precipitation of silica from pore waters or input of biogenic silica is probable (Uffmann et al., 2012). A discussion on the origin of secondary silica is given in chapter 4.5.

In contrast to MFT-1, the mineralogy of MFT-2 shows higher amounts of illite and mica, accounting for over 40% of the sample. In this microfacies, quartz contents are relatively low with 50% and less. Carbonate content in these samples are absent with the exception of a dolomitized sample with 69% Fe-dolomite (see Fig. 7).

The only XRD sample of a representative for MFT-3 shows the same mineralogical composition with the exception of up to 10% calcite originating from bioclasts (see 4.1.3). Due to the changing amounts of calcareous bioclasts observed within petrographic thin sections of MFT-3 (see 4.1.3), it has to be noted that this sample is not representative for the mineralogical facies characteristics of MFT-3.

4.4.2 Mineralogical facies characteristics of locality 2

While MFT-4 and MFT-5 show differences in microfacies analysis (see 4.2.2) and elemental organic geochemistry (see 4.3.2), the mineralogical composition of these microfacies types is the same (Fig. 7). Both microfacies types show clay and mica contents of over 60%, the highest values of all microfacies observed. Additionally, while the samples from locality 1 have low amounts of chlorite (< 3%); MFT-4 and MFT-5 contain increased, but varying amounts of chlorite (5 – 19%). Very small contents of siderite (c. 1%) constitute the carbonate fraction of these facies types.

The mineralogical composition of MFT-6 generally resembles the one of MFT-2 from locality 1. Differences are seen within the

carbonate fraction that consists of siderite and calcite constituting up to 8% of the total rock mineralogical composition. Moreover, within MFT-6, the moderate clay contents are equally distributed between illite/mica and chlorite while the clay fraction of MFT-2 almost exclusively consists of illite/mica. With regard to the high maturity of the samples, a diagenetic origin of this chlorite (Jennings & Thompson, 1986) may be assumed, but is unlikely because there is no relevant evidence given by SEM observations. In addition, all samples of higher maturity from locality 1 show very low amounts of chlorite, leading to the assumption that the majority of chlorite at locality 2 is of detrital origin as well.

4.5 Effects of diagenesis on mineral assemblage

Due to the suspiciously high quartz mineral values obtained from XRD of the different mudstone facies types, especially for locality 1, selected mudstone samples from both localities were investigated by SEM (Fig. 8). Results show that all mudstones, independent from facies, are influenced by secondary silica formation. In the case of apparently silicified samples ("phtanites"), authigenic silica formation likewise comprises components and matrix. Authigenic silica growth of mudstones that lacks a strong macroscopic silicification is expressed by a zoned overgrowth of detrital quartz grains, independent from grain-size. These observations show that interpreting XRD results without further information may lead to an overestimation of detrital quartz content. However, the question of the authigenic silica source still remains.

Silica dissolution and re-precipitation of quartz grains by acidic pore waters can be excluded because the nucleus of silica-overgrown grains still shows an angular and thus uninfluenced appearance, typical for detrital grains. Within marginal basin

settings, i.e. the Chokier Formation, terrigenous clastic deposition dominates and biogenic silica will be of little consequence for the total sediment budget (Schieber et al., 2000).

In situ quartz silt formation within organic-walled casings (e.g. algal cysts; spore casings) that served as a mold for silica precipitation has been observed only once within the investigated mudstones (Fig. 8B). Schieber et al. (2000) claimed a biogenic source for "in situ" quartz silt formation. Although silica of biogenic origin has been observed on specific levels in the basal Chokier Formation (Bellière, 1920) we do not have any proof of relevant fossil specimens, e.g. radiolarians and sponge spicules in our material neither by thin section petrography nor by SEM. Thus, the source of silica remains obscure. According Laschet (1984) a high supply rate of terrestrially dissolved silica to oceans can explain the formation of silica-rich pore waters and corresponding formation of siliceous deposits, as well as the silicification processes in unconsolidated sedimentary rocks. A high supply rate of terrestrially dissolved silica to oceans may be explained by the drowning karst topography that was covered by acidic soils.

5. Conclusions

By the example of two wells from the Namur Synclinorium six mudstone facies types could be identified for the Chokier Formation. The facies types of locality 1 (MFT-1, laminated silty mudstone; MFT-2, laminated mud-clast-rich mudstone; MFT-3, calcareous bioclast-rich mudstone) and locality 2 (MFT-4, lenticular mudstone; MFT-5, burrow-mottled mudstone; MFT-6, burrowed silty laminated mudstone) comprise common sedimentary features indicating a paleoenvironment that is

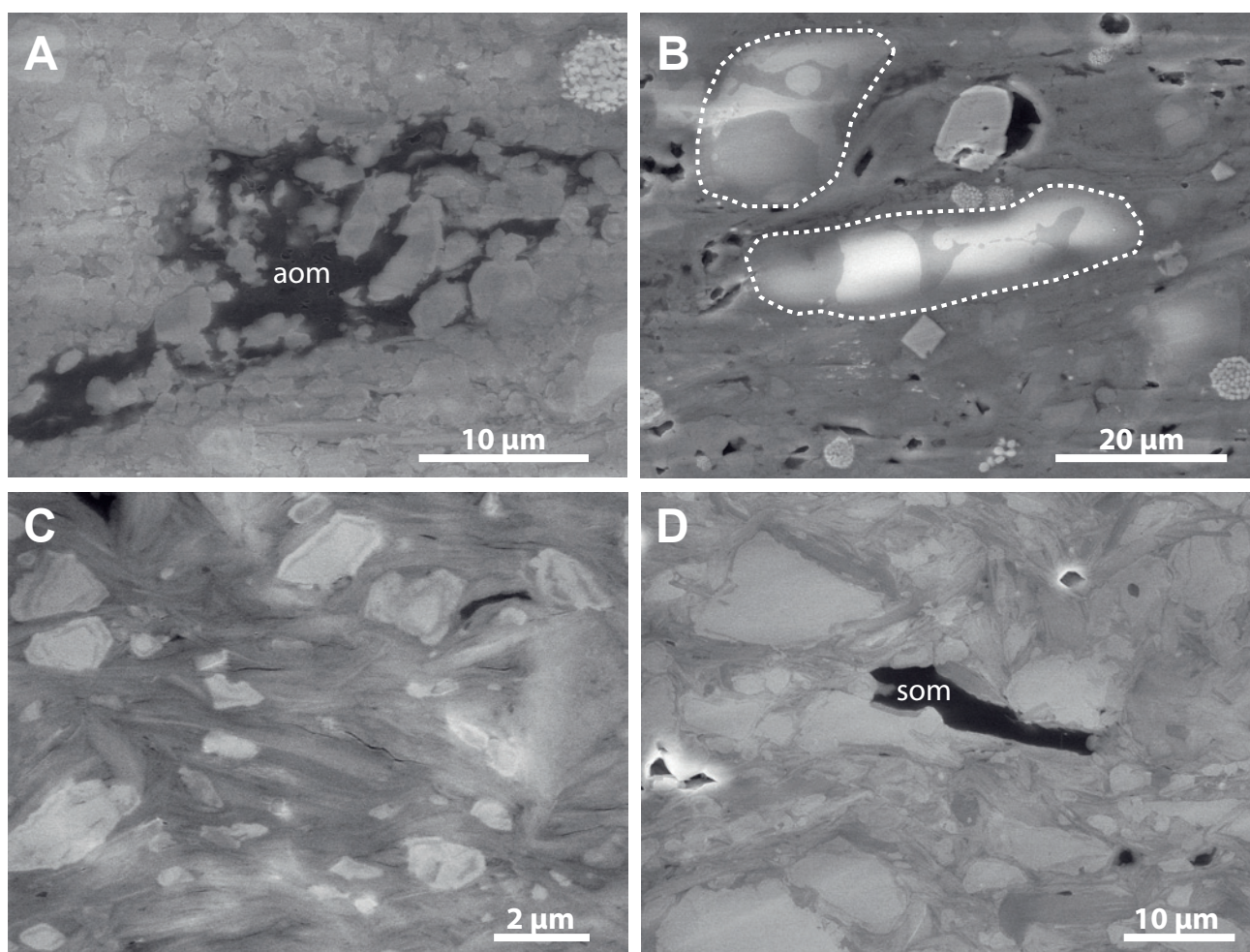


Figure 8. Examples of authigenic silica formation seen under SEM for locality 1 (A; B) and locality 2 (C; D). A: Example of a laminated silty mudstone (MFT-1) (see 4.1.1) with a high amount of authigenic silica. Note authigenic silica within amorphous organic matter-filled pore space (aom). B: Example of a laminated mud-clast-rich mudstone (MFT-2) (see 4.1.2) showing in-situ silica formation within two organic-walled casings (dashed lines). C: Example of a lenticular mudstone (MFT-4) (see 4.2.1) with diagenetic silica growth around detrital quartz grains. D: Structured organic matter (som) within a matrix of a burrowed silty laminated mudstone (MFT-6) (see 4.2.3) that is rich in detrital quartz, overgrown by thin layers of diagenetic silica.

assumed to be mainly sourced by erosive bedload. Accumulation by settling from the water column is of minor importance.

Various, but simple ichnofabrics show that oxygen conditions were highly variable and certain benthic colonization by soft-bodied organism that lack a calcitic shell was, at least temporarily favored. This is in very good accordance with TS/TOC ratios. Especially lower TS/TOC ratios confirm a (temporary) oxygenated seafloor for MFT-5 and the silt-rich MFT-6. The latter is restricted to the upper unit of locality 2 and is assumed to reflect the transition to the overlying paralic and coal-bearing Andenne Formation.

Organic matter preservation most likely is linked with high sedimentation rates, rather than extensive anoxicity. In contrast, highest TOC values, observed in locality 1 correlate with occurrence of MFT-2 and MFT-3 that in turn correlate with occurrence of goniatites. This might indicate a high sea level under fully marine conditions and TOC accumulation by reduced dilution of siliciclastic material due to lowered sedimentation rates and enhanced organic matter productivity. Apart from the high marine organic matter input, a certain terrestrial contribution (plant remains) is most likely.

SEM observations and sedimentary features show that silicification is possibly linked to a high supply rate of terrestrially dissolved silica. Biogenic silica is of minor importance. Although silicification is highly variable and independent from facies, it is a ubiquitous feature for the mudstones of the Chokier Formation, especially for locality 1. This demonstrates the necessity of a multidisciplinary approach for correct interpretation of quartz content obtained by XRD.

Facies assemblage of both localities is different and comprises also distinct features in elemental organic geochemistry and mineralogy. In particular, larger grain-sizes, significantly reduced amount of calcareous material, increased amount of detrital accumulations, i.e. sand- and siltstones, and high chlorite values hint to substantially different sediment sources or depositional mechanisms for locality 2. These features suggest that locality 2 was relatively more proximal compared to locality 1. Regarding the Arnsbergian age of locality 1 and the younger Chokierian age of locality 2, the distal to proximal depositional scenario may reflect a gradual facies development through time.

Due to the local occurrence of high-energy shallow-water crinoidal rudstone (Tramaka Member) close to the base of the formation and the paleokarstic features of underlying Viséan limestones a rather shallow environment for the basal Chokier Formation, i.e. locality 1 is assumed. Although the uppermost part, i.e. locality 2 apparently reflects a quite shallow depositional environment, especially with regard to a gradual transition to overlying coal bearing strata, a distal shelf environment below storm wave base seems to be realistic for the main part of the investigated Chokier Formation. Considering the paleotopography of a sea invading the land in between topographic highs, and the island (or peninsula) character of the proximal land, even wave action would be negligible. This leads to the assumption that the observed rapid accumulation of terrigenous clastic deposits to sea is linked to seasonal (monsoonal) transport.

6. Acknowledgements

CJN acknowledges Wintershall Holding GmbH for providing a unique forum of interdisciplinary scientific work and financial support. Additional financial support to CJN from the Graduate School of Geosciences University of Cologne is gratefully acknowledged. Furthermore, he also likes to thank Prof. Dr. J. Schieber for discussions of inestimable value and supervision at IU Shale Research Center SEM laboratory. Prof. Dr. H.-G. Herbig is acknowledged for reviewing an earlier version of the manuscript. Prof. Dr. R. Littke kindly provided access to laboratory equipment of the RWTH Aachen. R. Bäumler is thanked for technical assistance at the University of Cologne. Additional gratitude is extended to Prof. Dr. R. Swennen and Carmeuse S.A., in particular Marie Sautois, for providing access to important core material. Finally, we would like to thank Prof. Dr. R. Swennen, Dr. B. Delcambre and Dr. M. Dusar for their constructive reviews.

7. References

- Ancion, C. & Van Leckwijck, W., 1947. Contribution à l'étude de la stratigraphie du Bassin d'Andenne: niveaux gréseux et horizons marins du Namurien. *Annales de la Société géologique de Belgique*, 70, 266-306.
- Andrews, I.J., 2013. The Carboniferous Bowland Shale gas study: geology and resource estimation. British Geological Survey for Department of Energy and Climate Change, London, UK.
- Anten, J. & Bellière, M., 1920. Sur les phatanites de la base du houillier inférieur au bord nord du bassin de Namur à Horion-Hozémont. *Annales de la Société géologique de Belgique*, 43, B127-130.
- Austin, R., Conil, R., Groessens, E. & Pirllet, H., 1974. Etude biostratigraphique de l'encrinite de Tramaka. *Bulletin de la Société belge de Géologie, de Paléontologie et d'Hydrologie*, 83, 113-129.
- Banerjee, S., Dutta, S., Paikaray, S. & Mann, U., 2006. Stratigraphy, sedimentology and bulk organic geochemistry of black shales from the Proterozoic Vindhyan Supergroup (central India). *Journal of Earth System Science*, 115, 37-47.
- Belanger, I., Delaby, S., Delcambre, B., Ghysel, P., Hennebert, M., Laloux, M., Marion, J. M., Mottequin, B. & Pingot, J.-L., 2012. Redéfinition des unités structurales du front varisque utilisées dans le cadre de la nouvelle Carte géologique de Wallonie (Belgique). *Geologica Belgica*, 15, 169-175.
- Bellièvre, M., 1920. L'existence du spongolithes dans le houiller inférieur. *Annales de la Société géologique de Belgique*, 43, B115-127.
- Berner, R.A., 1984. Sedimentary pyrite formation: an update. *Geochimica et Cosmochimica Acta*, 48, 605-615.
- Blatt, H., 1992. *Sedimentary Petrology*. Freeman and Co., New York.
- Bouckaert, J., 1967. Namurien transgression in Belgium. *Rocznik Polskiego Towarzystwa Geologicznego (Annales de la Société géologique de Pologne)*, 37, 145-150.
- Bouckaert, J. & Lambrecht, L., 1967. Le Namurien du flanc sud du synclinal de Liège entre Seraing et Amay (province de Liège). *Bulletin de la Société belge de Géologie*, 75, 7-27.
- Davies, S.J., Leng, M.J., Macquaker, J.H.S. & Hawkins, K., 2012. Sedimentary process control on carbon isotope composition of sedimentary organic matter in an ancient shallow-water shelf succession. *Geochemistry, Geophysics, Geosystems*, 13, 1525-2027.
- Davydov, V.I., Korn, D. & Schmitz, M.D., 2012. The Carboniferous Period. In Gradstein, F., Ogg, J., Schmitz, M., & Ogg, G., (eds), *The Geological Time Scale*. Amsterdam, Elsevier, 603-651.
- de Béthune, P., 1954. Carte géologique de Belgique (échelle 1/500.000; planche 8). Atlas de Belgique. Académie royale de Belgique, Brussels.
- Delmer, A., Dusar, M. & Delcambre, B., 2001. Upper Carboniferous lithostratigraphic units (Belgium). *Geologica Belgica*, 4, 95-103.
- Devuyt, F.-X., Hance, L. & Poty, E., 2005. The Dinantian of Southern Belgium revisited: sedimentary history and biostratigraphy. A guidebook of key sections. I.U.G.S. Subcommittee on Carboniferous Stratigraphy field trip, May 2005: 1-79.
- Dusar, M., 2006a. Chokierian. *Geologica Belgica*, 9, 177-187.
- Dusar, M., 2006b. Namurian. *Geologica Belgica*, 9, 163-175.
- Gabbott, S.E., Zalasiewicz, J., Aldridge, R.J. & Theron, J.N., 2010. Eolian input into the Late Ordovician postglacial Soom Shale, South Africa. *Geology*, 38, 1103-1106.
- Gerrienne, P., Fairon-Demaret, M. & Galtier, J., 1999. A Namurian A (Silesian) permineralized flora from the Carrière du Lion at Engihoul (Belgium). *Review of Palaeobotany and Palynology*, 107, 1-15.
- Ghanizadeh, A., Gasparik, M., Amann-Hildenbrand, A., Gensterblum, Y. & Krooss, B.M., 2013. Lithological Controls on Matrix Permeability of Organic-rich Shales: An Experimental Study. *Energy Procedia*, 40, 127-136.
- Hance, L., Poty, E. & Devuyt, F.-X., 2001. Stratigraphie séquentielle du Dinantien type (Belgique) et corrélation avec le Nord de la France (Boulonnais, Avesnois). *Bulletin de la Société géologique de France*, 172, 411-426.
- Hartwig, A., Könitzer, S., Boucsein, B., Horsfield, B. & Schulz, H.-M., 2010. Applying classical shale gas evaluation concepts to Germany — Part II: Carboniferous in Northeast Germany. *Chemie der Erde*, 70, 93-106.
- Hovikoski, J., Lemiski, R., Gingras, M., Pemberton, G. & MacEachern, J. A., 2008. Ichnology and Sedimentology of a Mud-Dominated Deltaic Coast: Upper Cretaceous Alderson Member (Lea Park Fm), Western Canada. *Journal of Sedimentary Research*, 78, 803-824.
- Jennings, S. & Thompson, G.R., 1986. Diagenesis of Plio-Pleistocene Sediments of the Colorado River Delta, Southern California. *Journal of Sedimentary Petrology*, 56, 89-98.
- Kerschke, D. & Schulz, H.-M., 2013. The shale gas potential of Tournaisian, Viséan, and Namurian black shales in North Germany: baseline parameters in a geological context. *Environmental Earth Sciences*, 70, 3817-3837.

- Knaust, D.K., 2002. Pinch-and-swell structures at the Middle/Upper Muschelkalk boundary (Triassic): evidence of earthquake effects (seismites) in the Germanic Basin. *International Journal of Earth Sciences*, 91, 291-303.
- Kombrink, H., Leever, K.A., Van Wees, J.-D., Van Bergen, F., David, P. & Wong, T.E., 2008. Late Carboniferous foreland basin formation and Early Carboniferous stretching in Northwestern Europe: inferences from quantitative subsidence analyses in the Netherlands. *Basin Research*, 20, 377-395.
- Könitzer, S.F., Davies, S.J., Stephenson, M.H. & Leng, M.J., 2014. Depositional Controls On Mudstone Lithofacies in a Basinal Setting: Implications for the Delivery of Sedimentary Organic Matter. *Journal of Sedimentary Research*, 84, 198-214.
- Korn, D., 2006. Lithostratigraphische Neugliederung der Kulm-Sedimentgesteine im Rheinischen Schiefergebirge. In *Deutsche Stratigraphische Kommission (eds), Stratigraphie von Deutschland VI. Unterkarbon (Mississippium)*. Schriftenreihe der deutschen Gesellschaft für Geowissenschaften, Hannover, 41, 379-383.
- Langenaeker, V. & Dusar, M., 1992. Subsurface facies analysis of the Namurian and earliest Westphalian in the western part of the Campine Basin (N. Belgium). *Geologie en Mijnbouw*, 71, 161-172.
- Laschet, C., 1984. On the origin of cherts. *Facies*, 10, 257-289.
- Littke, R., Krooss, B., Uffmann, A.K., Schulz, H.-M. & Horsfield, B., 2011. Unconventional Gas Resources in the Paleozoic of Central Europe. *Oil and Gas Science Technology – Review IFP Energies nouvelles*, 66, 953-977.
- Littke, R., Urai, J.L., Uffmann, A.K. & Risvanis, F., 2012. Reflectance of dispersed vitrinite in Palaeozoic rocks with and without cleavage: Implications for burial and thermal history modeling in the Devonian of Rursee area, northern Rhenish Massif, Germany. *International Journal of Coal Geology*, 89, 41-50.
- MacEachern, J.A., Pemberton, S.G., Bann, K.L. & Gingras, M.K., 2009. Departures from the archetypal ichnofacies: Effective recognition of Physio-Chemical stresses in the Rock record. In MacEachern, J.A., Bann, K.L., Gingras, M.K. & Pemberton, S.G. (eds), *Applied Ichnology. SEPM Short Course Notes*, 52, Tulsa, 65-94.
- Macquaker, J.H.S., Keller, M.A. & Davies, S. J., 2007. Algal Blooms and “Marine Snow”: Mechanisms that Enhance Preservation of Organic Carbon in Ancient Fine-Grained Sediments. *Journal of Sedimentary Research*, 80, 934-942.
- Maynard, J. R. & Dunay, R.E., 1999. Reservoirs of the Dinantian (Lower Carboniferous) play of the Southern North Sea. In Fleet, A.J. & Boldy, S.A.R. (eds), *Petroleum Geology of Northwest Europe: Proceedings of the 5th Conference*. London, Geological Society, 729-745.
- Milliken, K., Choh, S.-J., Papazis, P. & Schieber, J., 2007. „Cherty“ stringers in the Barnett Shale are agglutinated foraminifera. *Sedimentary Geology*, 198, 221-232.
- Muchez, P., Viaene, W., Wolf, W. & Bouckaert, J., 1987. Sedimentology, coalification pattern and paleogeography of the Campine-Brabant Basin during the Viséan. *Geologie en Mijnbouw*, 66, 313-326.
- Nyhuys, C.J., Amler, M.R.W. & Herbig, H.-G., submitted. Facies and palaeoecology of the late Viséan (Mississippian) *Actinopteria* Black Shale Event in the Rhenish Mountains (Germany). *Zeitschrift der Deutschen Gesellschaft für Geowissenschaften*.
- Paproth, E., Dusar, M., Bless, M.J.M., Bouckaert, J., Delmer, A., Fairon-Demaret, M., Houllberghs, E., Laloux, M., Pierart, P., Somers, Y., Streel, M., Thorez, J. & Tricot, J., 1983. Bio- and lithostratigraphic subdivisions of the Silesian in Belgium, a review. *Annales de la Société géologique de Belgique*, 106, 241-283.
- Pemberton, S.G., MacEachern, J.A., Gingras, M.K. & Saunders, T.D.A., 2008. Biogenic chaos: Cryptobioturbation and the work of sedimentologically friendly organisms. *Palaeogeography, Palaeoclimatology, Palaeoecology*, 270, 273-279.
- Piper, D.J.W. & Stow, D.A.V., 1991. Fine-Grained Turbidites. In Einsele, G., Ricken, W. & Seilacher, A. (eds), *Cycles and Events in Stratigraphy*. Heidelberg, Springer-Verlag, 361-376.
- Poty, E., Aretz, M. & Denayer, J., 2011. Field trip 3: Uppermost Devonian and Lower Carboniferous of Southern Belgium. In Aretz, M. & Poty, E. (eds), *11th International Symposium on Fossil Cnidaria and Porifera - Liège*, 19-29 August, 2011, Field-Guides. *Kölner Forum für Geologie und Paläontologie*, 20, 99-150.
- Rodríguez-Tovar, F.J. & Uchman, A., 2010. Ichnofabric evidence for the lack of bottom anoxia during the lower Toarcian. Oceanic Anoxic Event in the Fuente de la Vidriera section, Betic Cordillera, Spain. *Palaios*, 25, 576-587.
- Rullkötter, J., Leythaeuser, D., Horsfield, B., Littke, R., Mann, U., Müller, P.J., Radke, M., Schaefer, R.G., Schenk, H.-J., Schwochau, K., Witte, E.G. & Welte, D.H., 1988. Organic matter maturation under the influence of a deep intrusive heat source: A natural experiment for quantitation of hydrocarbon generation and expulsion from a petroleum source rock (Toarcian shale, northern Germany). In Mattavelli, L. & Novelli, L. (eds), *Advances in Organic Geochemistry 1987*. Oxford, Pergamon Press, 847-856.
- Sachse, V.F., Littke, R., Heim, S., Kluth, O., Schober, J., Boutib, L., Jabour, H., Perssen, F. & Sindern, S., 2011. Petroleum Source Rocks of the Tarfaya Basin and adjacent areas, Morocco. *Organic Geochemistry*, 42, 209-227.
- Schieber, J., 2009. Discovery of agglutinated benthic foraminifera in Devonian black shales and their relevance for the redox state of ancient seas. *Palaeogeography Palaeoclimatology Palaeoecology*, 271, 292-300.
- Schieber, J., Krinsley, D. & Riciputi, L., 2000. Diagenetic origin of quartz silt in mudstones and implications for silica cycling. *Nature*, 406, 981-985.
- Schieber, J., Southard, J.B. & Schimmelmann, A., 2010. Lenticular Shale Fabrics Resulting from Intermittent Erosion of Muddy Sediments – Comparing Observations from Flume Experiments to the Rock Record. *Journal of Sedimentary Research*, 80, 119-128.
- Schieber, J., Sur, S. & Banerjee, S., 2007. Benthic microbial mats in black shale units from the Vindhyan Supergroup, Middle Proterozoic of India: the challenges of recognizing the genuine article. In Schieber, J., Bose, P. K., Eriksson, P. G., Banerjee, S., Sarkar, S., Altermann, W. & Catuneau, O. (eds), *Atlas of Microbial Mat Features Preserved within the Siliciclastic Rock Record*. Amsterdam, Elsevier, 189-197.
- Schoenherr, J., Littke, R., Urai, J.L., Kukla, P.A. & Rawahi, Z., 2007. Polyphase thermal evolution in the Infra-Cambrian Ara Group (South Oman Salt Basin) as deduced by maturity of solid reservoir bitumen. *Organic Geochemistry*, 38, 1293-1318.
- Seilacher, A., 1967. Biogenic sedimentary structures. In Imbrie, J. & Newell, N. (eds), *Approaches to paleoecology*. New York, Wiley, 296-316.
- Taylor, G.H., Teichmüller, M., Davis, A., Diessel, C.F.K., Littke, R. & Robert, P., 1998. *Organic petrology*. Gebrüder Borntraeger, Berlin.
- Tourtlot, H. A., 1979. Black Shales — its deposition and diagenesis. *Clays and Clay Minerals*, 27, 313-321.
- Trabucho-Alexandre, J., Dirkx, R., Veld, H., Klaver, G. & de Boer, P.L., 2012. Toarcian Black Shales In the Dutch Central Graben: Record of Energetic, Variable Depositional Conditions During an Oceanic Anoxic Event. *Journal of Sedimentary Research*, 82, 104-120.
- Uffmann, A.K., Littke, R. & Rippen, D., 2012. Mineralogy and geochemistry of Mississippian and Lower Pennsylvanian Black Shales at the Northern Margin of the Variscan Mountain Belt (Germany and Belgium). *International Journal of Coal Geology*, 103, 92-108.
- Van Hulst, F.F.N., 2012. Devonian-Carboniferous carbonate platform systems of the Netherlands. *Geologica Belgica*, 15, 284-296.
- Van Hulst, F.F.N. & Poty, E., 2008. Geological factors controlling Early Carboniferous carbonate platform development in the Netherlands. *Geological Journal*, 43, 175-196.
- Van Leckwijck, W. & Stockmans, F., 1956. La limite entre les assises namuriennes d'Andenne et de Chokier. *Bulletin de la Société belge de Géologie, de Paléontologie et d'Hydrologie*, 65, 292-306.
- Van Leckwijck, W., 1964. Le Namurien en Belgique et dans les régions limitrophes (Stratigraphie, Paléogéographie, Paléontologie, Sédimentologie, Puissances). *Mémoires de l'Académie royale de Belgique, Classe des Sciences, deuxième série*, 16, 1-58.
- Wetzel, A., 1983. Biogenic structures in modern slope to deep-sea sediments in the Sulu Sea Basin (Philippines). *Palaeogeography, Palaeoclimatology, Palaeoecology*, 42, 285-304.
- Wetzel, A. & Uchmann, A., 1998. Biogenic Sedimentary Structures in Mudstones - an Overview. In Schieber, J., Zimmerle, W. & Sethi, P. (eds), *Shales and Mudstones. E Schweizerbart'sche, Volume 1*, Stuttgart, 351-369.